HIF-2 Complex Dissociation, Target Inhibition, and Acquired Resistance with PT2385, a First-in-Class HIF-2 Inhibitor, in Patients with Clear Cell Renal Cell Carcinoma

Kevin D. Courtney[1,2], Yuanqing Ma[1,2], Alberto Diaz de Leon[2,3], Alana Christie[2], Zhiqun Xie[2,4], Layton Woolford[1,2], Nirmish Singla[2,5], Allison Joyce[1,2], Haley Hill[1,2], Ananth J. Madhuranthakam[2,3], Qing Yuan[2,3], Yin Xi[3,4], Yue Zhang[3], Jenny Chang[1,2], Oluwatomilade Fatunde[1,2], Yull Arriaga[1,2], Arthur E. Frankel[1,2], Sanjeeva Kalva[3], Song Zhang[2,6], Tiffani McKenzie[2,7], Oscar Reig Torras[2], Robert A. Figlin[8], Brian I. Rini[9], Renée M. McKay[1,2], Payal Kapur[2,7], Tao Wang[2,4], Ivan Pedrosa[2,3], and James Brugarolas[1,2]

ABSTRACT

Purpose: The heterodimeric transcription factor HIF-2 is arguably the most important driver of clear cell renal cell carcinoma (ccRCC). Although considered undruggable, structural analyses at the University of Texas Southwestern Medical Center (UTSW, Dallas, TX) identified a vulnerability in the α subunit, which heterodimerizes with HIF1β, ultimately leading to the development of PT2385, a first-in-class inhibitor. PT2385 was safe and active in a first-in-human phase I clinical trial of patients with extensively pretreated ccRCC at UTSW and elsewhere. There were no dose-limiting toxicities, and disease control ≥4 months was achieved in 42% of patients.

Patients and Methods: We conducted a prospective companion substudy involving a subset of patients enrolled in the phase I clinical trial at UTSW ($n = 10$), who were treated at the phase II dose or above, involving multiparametric MRI, blood draws, and serial biopsies for biochemical, whole exome, and RNA-sequencing studies.

Results: PT2385 inhibited HIF-2 in nontumor tissues, as determined by a reduction in erythropoietin levels (a pharmacodynamic marker), in all but one patient, who had the lowest drug concentrations. PT2385 dissociated HIF-2 complexes in ccRCC metastases, and inhibited HIF-2 target gene expression. In contrast, HIF-1 complexes were unaffected. Prolonged PT2385 treatment resulted in the acquisition of resistance, and we identified a gatekeeper mutation (G323E) in HIF2α, which interferes with drug binding and precluded HIF-2 complex dissociation. In addition, we identified an acquired *TP53* mutation elsewhere, suggesting a possible alternate mechanism of resistance.

Conclusions: These findings demonstrate a core dependency on HIF-2 in metastatic ccRCC and establish PT2385 as a highly specific HIF-2 inhibitor in humans. New approaches will be required to target mutant HIF-2 beyond PT2385 or the closely related PT2977 (MK-6482).

Introduction

Clear cell renal cell carcinoma (ccRCC) is characterized by inactivation of the tumor suppressor gene, von Hippel-Lindau (*VHL*), which occurs in the majority of tumors (1). pVHL functions as the substrate recognition subunit of an E3 ubiquitin ligase complex that targets the α subunit of the heterodimeric hypoxia-inducible factor (HIF) transcription factor for degradation (2). When *VHL* is inactivated, HIFα constitutively accumulates, binds the HIF1β subunit (also called ARNT), and induces downstream gene expression (3). Among the three known HIFα subunits, HIF2α is believed to be the critical ccRCC driver (4–6). The HIF-2 complex promotes the expression of over 100 proteins including VEGF (VEGFA), which binds VEGF receptor-2 (VEGFR2) on endothelial cells to promote angiogenesis (7). ccRCC is characterized by high levels of VEGF (8), and multiple inhibitors of VEGF/VEGFR2 are approved for the treatment of advanced ccRCC (9).

In addition to VEGF, HIF-2 also stimulates cell cycle progression and maintains stemness, which likely contribute to tumorigenesis (4, 10). Thus, inhibiting HIF-2 would not only target the pathway more proximally, but also more broadly. However, as a transcription factor, HIF-2 has traditionally been regarded as undruggable (11). Nevertheless, structural analyses at UT Southwestern Medical Center (UTSW, Dallas, TX) identified a vulnerability in the PAS-B domain of HIF2α, which paved the way for the identification of small-molecule inhibitors (12, 13). These inhibitors induce a conformational change in the PAS-B domain, which interferes with the

[1]Hematology-Oncology Division, Department of Internal Medicine, University of Texas Southwestern Medical Center, Dallas, Texas. [2]Kidney Cancer Program, Simmons Comprehensive Cancer Center, University of Texas Southwestern Medical Center, Dallas, Texas. [3]Department of Radiology, University of Texas Southwestern Medical Center, Dallas, Texas. [4]Department of Population and Data Sciences, Quantitative Biomedical Research Center, University of Texas Southwestern Medical Center, Dallas, Texas. [5]Department of Urology, University of Texas Southwestern Medical Center, Dallas, Texas. [6]Department of Population and Data Sciences, University of Texas Southwestern Medical Center, Dallas, Texas. [7]Department of Pathology, University of Texas Southwestern Medical Center, Dallas, Texas. [8]Division of Hematology/Oncology, Cedars-Sinai Medical Center, Los Angeles, California. [9]Department of Hematology and Medical Oncology, Cleveland Clinic, Cleveland, Ohio.

Note: Supplementary data for this article are available at Clinical Cancer Research Online (http://clincancerres.aacrjournals.org/).

K.D. Courtney, Y. Ma, and A. Diaz de Leon contributed equally to this article.

Current address for A.E. Frankel: West Palm Beach VA Medical Center, West Palm Beach, Florida.

Corresponding Authors: Ivan Pedrosa, University of Texas Southwestern Medical Center, 5323 Harry Hines Blvd., Dallas, TX, 75390-9085. Phone: 214-645-2285; Fax: 214-648-7785. E-mail: ivan.pedrosa@utsouthwestern.edu; and James Brugarolas, University of Texas Southwestern Medical Center, 5323 Harry Hines Blvd., Dallas, TX 75390-8852. Phone: 214-648-4059; Fax: 214-648-1955; E-mail: james.brugarolas@utsouthwestern.edu

Clin Cancer Res 2020;26:793–803

doi: 10.1158/1078-0432.CCR-19-1459

Translational Relevance

We report that a first-in-class, first-in-human, HIF2α inhibitor (PT2385) effectively inhibits HIF-2 both in nontumor as well as tumor tissues, leading to the dissociation of HIF-2 complexes, and the inhibition of target genes. This effect is specific for HIF-2, and HIF-1 complexes were unaffected. We identify, for the first time in humans, a resistance mutation, which validates HIF2α as the drug target, and reveals a fundamental dependency on HIF-2 for tumor progression. This study establishes a core dependency in ccRCC that may be further exploited therapeutically.

assembly of HIF2α/HIF1β heterodimers (14). These inhibitors led to the development of PT2385 by Peloton Therapeutics, Inc., in the UTSW BioCenter (and the highly related tool compound, PT2399; refs. 15–17). PT2385 was evaluated in a phase I dose escalation/expansion clinical trial, where it was found to be well-tolerated and showed clinical activity (18). Among 51 patients in the trial, 21 patients had disease control for at least 4 months. However, whether PT2385 effectively inhibits HIF-2 in patients with ccRCC, how specific the effect is, and the overall importance of HIF-2 in ccRCC progression is poorly understood.

Patients and Methods

Study design and participants

This was a prospective, nontherapeutic pilot imaging and biomarker companion study approved by IntegReview Institutional Review Board (IRB) at UTSW (STU 062015-063), involving a subset of patients in the phase I clinical trial "Phase I, Multiple-Dose, Dose-Escalation Trial of PT2385 Tablets, a HIF-2α Inhibitor, in Patients with Advanced Clear Cell Renal Cell Carcinoma (NCT02293980)." All patients in this companion study were enrolled in the phase I trial at UTSW, and all were treated at the recommended phase II dose or above. This companion trial was performed in accordance with the Declaration of Helsinki and approved by the IRB. All patients provided written informed consent. Patients with advanced or metastatic ccRCC who consented to the phase I trial of PT2385 and were treated at UTSW were eligible. The study involved several interventions, including contrast-enhanced MRI, which required an estimated glomerular filtration rate (eGFR) $\geq$30 mL/minute/1.73m^2 and at least one candidate intra-abdominal, intrathoracic, or osseous lesion >2.5 cm. Subjects who had a contraindication to magnetic resonance imaging (MRI) could still participate in the blood collection and optional tumor biopsy portions of this study. Patient identification numbers are chronologic and were those assigned for the phase I trial (18). Patient samples were also collected as part of a UTSW IRB-approved tissue collection protocol ("Kidney Cancer New Pathway Discovery Project," STU 012011-190). Descriptive data are presented and includes weeks on treatment as well as progression-free survival (PFS), which may differ slightly depending upon when drug was stopped.

Procedures

Multiparametric MRI (mpMRI) was performed and blood samples were collected during screening, on treatment (at 2, 6–7, and 16 weeks), and at progression. Optional core tumor biopsies were performed during screening, on treatment (at weeks 6–7), and at progression. Additional core biopsies could be obtained from a responding or progressing lesion at one additional time point while the patient was on treatment. Erythropoietin (EPO) levels and plasma concentration of PT2385 were measured by Peloton Therapeutics as part of the phase I trial (18).

MRI protocol and analyses

All exams were performed on a 3T MRI scanner (Philips) using a phased-array surface coil. Coronal and axial T2-weighted imaging, axial diffusion-weighted imaging (DWI), and coronal dynamic contrast-enhanced (DCE) acquisitions were obtained through the abdomen (Supplementary Table S1). DCE MRI was performed with a three-dimensional (3D) T1-weighted (T1W) spoiled gradient-echo (SPGR) acquisition before, during, and after the intravenous administration of 0.1 mmol/kg of gadobutrol (Gadavist; Bayer Healthcare Pharmaceuticals) at a rate of 2 mL/second followed by a 20-mL saline flush at 2 mL/second. Images were obtained for a total of 6 minutes and 15 seconds with a 5-second temporal resolution. Three dynamic phases were acquired during breath-hold intervals with 15-second free-breathing cycles. To generate a T1 map, three additional coronal 3D T1W SPGR acquisitions were obtained prior to the administration of contrast using the same acquisition parameters as those of the DCE MRI acquisition except for flip angles of 10°, 5°, and 2°, respectively.

Two-dimensional arterial spin labeled (ASL) MRI was acquired prior to administration of contrast via pseudo-continuous labeling of the abdominal aorta as described previously (ref. 19; Supplementary Table S1). ASL images were prescribed in the axial or coronal plane by a fellowship-trained radiologist with expertise in MRI (I. Pedrosa, 17 years of experience) to cover the center of each target lesion.

mpMRI acquisition parameters for ASL, DCE, and DWI are presented in Supplementary Table S1. DCE images were processed using a commercial software (VersaVue, iCAD Inc.) to generate quantitative maps of K^{trans} and K_{ep} from the extended Tofts model (20). ASL perfusion difference and quantitative perfusion maps were generated using Matlab (The MathWorks Inc.) as described previously (19). Apparent diffusion coefficient (ADC) maps ($\times 10^{-3}$ mm^2/sec) were generated using a mono-exponential model.

All MRI acquisitions were reviewed on an open-source Picture Archiving and Communication System workstation (OsiriX, Pixmeo). Regions of interest (ROI) were drawn by a fellowship-trained radiologist (A. Diaz de Leon, 5 years of experience) on the pretreatment mpMRI. Subsequent mpMRIs were analyzed by drawing ROIs in the same lesions using the baseline mpMRI as the reference for comparison. The radiologist was blinded to clinical data but unblinded to patient study ID. On the quantitative ASL perfusion maps, whole-lesion ROIs were drawn to outline the periphery of the lesion, avoiding the contour to minimize partial volume effects, to determine the mean perfusion level of the lesion in milliliters per minute per 100 g of tissue (mL/minute/100 g). Similar ROIs of the entire lesion were drawn on the DCE quantitative K^{trans} (min^{-1}) and K_{ep} (min^{-1}) maps, on a slice location that best matched the position of the ASL acquisition when feasible. On the ADC maps, a whole-lesion ROI was drawn on a single image that included the center of each target lesion. Data on DCE and DWI were not informative and are not included.

Sample nomenclature key

Nomenclature for tumor and tumorgraft identification is shown in Supplementary Table S2. Methods for generation of tumorgrafts and preclinical drug trials in mice were described previously (16, 21, 22).

List of abbreviations

Abbreviations are shown in Supplementary Table S3.

Proximity ligation assay

Proximity ligation assays (PLA) were performed as described previously (16). Mouse anti-HIF1α (NB100-105; Novus Biologicals), mouse anti-HIF2α (sc-46691X; Santa Cruz Biotechnology), and rabbit anti-ARNT/HIF1β (A302-765A; Bethyl Laboratories) were used. Primary antibodies were concentrated and buffers were exchanged using a Vivaspin 500 Centrifugal Concentrator (VS0131; Thermo Fisher Scientific). Antibodies were diluted to 1 mg/mL in PBS. Primary antibody conjugation was done with a Duolink In situ Probemaker MINUS/PLUS Kit (DUO92010 and DUO92009; Sigma-Aldrich). Briefly, 2 μL of conjugation buffer was added to 20 μL of the antibody (1 mg/mL), mixed gently, transferred to one vial of lyophilized oligonucleotide (PLUS or MINUS), and incubated at room temperature overnight. Two microliters of stop reagent was then added to the reaction and incubated at room temperature for 30 minutes. Storage solution (24 μL) was added and the conjugate was stored at 4°C. Tumor tissue was blocked with PBS-Triton (0.1% Triton X-100) + 1% BSA for 30 minutes after antigen retrieval. Conjugated HIF1α-MINUS, HIF2α-MINUS, and HIF1β-PLUS were diluted in blocking buffer containing 1× assay reagent at a dilution of 1:50, 1:50, and 1:200, respectively. The antibodies were allowed to sit for 20 minutes at room temperature before they were added to each sample. Slides were incubated in a humidity chamber overnight at 4°C. Duolink In situ Detection Reagents FarRed (DUO92013-30RXN; Sigma-Aldrich) were used for signal detection. Briefly, slides were washed with wash buffer A (catalog no. DUO82047; Sigma-Aldrich), a ligation solution containing ligase at a 1:40 was added, and slides were incubated in a preheated humidity chamber for 30 minutes at 37°C. After washing in buffer A with gentle agitation, amplification solution containing the polymerase was added at a 1:80 dilution, and slides were then incubated in a preheated humidity chamber for 100 minutes at 37°C. After washing in buffer B (catalog no. DUO82048; Sigma-Aldrich) and then 0.01 × buffer B, slides were dried at room temperature in the dark and mounted with a coverslip using a minimal volume of Duolink In situ Mounting Medium with DAPI (DUO82040; Sigma-Aldrich). After approximately 15 minutes, slides were analyzed by confocal microscopy (Nikon) using a 63× objective. Image analysis was done with the ImageJ 1.48V program, and performed blinded to the sample IDs. Pictures of three fields for each sample were used. At least 20 cells of each sample were counted. Pt27 samples were derived from touchpreps of an iliac mass biopsy pretreatment and then a biopsy of this same mass at week 6/7 on-treatment. Pt35 samples were derived from touchpreps of a liver tumor biopsy pretreatment and then a biopsy of this same mass at week 6/7 on-treatment. Pt45 samples were derived from touchpreps of a left adrenal mass biopsy pretreatment and then a biopsy of this same mass at week 6/7 on-treatment.

Whole-exome sequencing and mutation calling

Whole-exome sequencing (WES) was performed by Admera Health. DNA libraries were prepared using Integrated DNA Technologies xGen Lockdown Panel v1.0. Libraries were then sequenced at ≥100× coverage using Illumina's HiSeq 4000 with 150 bp pair-end reads. We used the Quantitative Biomedical Research Center (QBRC) mutation calling pipeline for somatic mutation calling, developed at UTSW (https://github.com/tianshilu/QBRC-Somatic-Pipeline). In short, exome-seq reads were aligned to the human reference genome (Hg38) by BWA-MEM (23). Picard was used to add read group information and sambamba was used to mark PCR duplicates. The Genome Analysis Toolkit was used to perform base quality score recalibration and local realignment around insertion/deletions (indels; refs. 24–26). MuTect, VarScan, Shimmer, SpeedSeq, Manta, and Strelka2 were used to call SNPs and indels (27–30). A mutation that was repeatedly called by any two of these software programs was retained. Annovar was used to annotate SNPs and indels, as well as protein sequence changes (31). All SNPs and indels were combined and only kept if there were at least seven total reads in the normal sample (wild-type and variant) and at least three variant reads in the tumor sample. Intronic, untranslated regions, and intergenic mutations were filtered out. Missense mutations predicted as benign by both PolyPhen-2 and Sorting Intolerant from Tolerant (SIFT), which have a <5% chance to induce functional changes at the protein level, were filtered out (32). Somatic mutations were annotated according to the variant allele frequencies in the normal (<5%) and tumor (>5% and at least two times larger than the variant allele frequency in the normal sample) samples. These studies were complemented through direct visualization of the mutated reads using the Integrated Genomics Viewer (IGV; Broad Institute). Color of the mutation depends upon the type of substitution.

Sequencing data for patients specifically consenting to have their genomic data shared in a public database will be deposited in the European Genome-phenome Archive under accession number EGAS00001003506.

RNA-sequence and analyses

mRNA was extracted from total RNA from flash frozen tumor tissue using NEBNext Poly(A) mRNA Magnetic Isolation Module Kits from New England BioLabs and library preparation was performed using Illumina's NEBNext Ultra RNA Library Prep Kit. Sequencing was performed at Admera Health Precision Medicine and Molecular Diagnostics Lab using Illumina's HiSeq4000 with average sequencing depth of 40M reads and 150 bp pair-end reads. FastQC (https://www.bioinformatics.babraham.ac.uk/projects/fastqc/) was applied to conduct quality control procedures, with the parameters "–extract –threads 48 -q." RNA-sequencing (RNA-seq) reads were aligned to the human reference genome GRCh38 (hg38) using STAR (33) with the parameters "–runThreadN 48 –outSAMtype BAM Unsorted –outReandsUnmapped Fastx." FeatureCounts (34) with parameters "–primary -O -t exon -g transcript_id -s 0 -T 48 –largestOverlap –minOverlap 3 –ignoreDup -p -P -B -C" was then used to measure gene expression levels. The human genome annotation file employed by FeatureCounts was downloaded from UCSC table browser under the RefSeq Gene track. Downstream analyses were performed in an R computing environment. Reads per kilobase million (RPKM) values were calculated from gene read counts. RPKM values were then $\log_2$-transformed and quantile normalized.

Gene signature enrichment analysis was carried out using the single sample gene set enrichment analysis (ssGSEA) method (35) given a set of signature genes (e.g., HIF-2 target signature). Specifically, ssGSEA analysis was performed using the R Gene Set Variation Analysis (GSVA) package by calling the gsva function with parameter method = "ssgsea" and rnaseq = T (36).

Statistical analyses

For mpMRI, planned analyses were mostly descriptive. We summarized continuous variables by mean, SD, and 95% confidence interval (CI), and categorical variables by frequency and percentage. We estimated intrapatient changes in tumor perfusion (by ASL), K^{trans} (by DCE), and ADC (by DWI), together with their 95% CIs. Median and 95% CI were used to report the response to PT2385 in terms of (i) RECIST 1.1, (ii) 10% reduction in sum of the longest one-dimensional

diameters (SLD), (iii) change in K^{trans}, and (iv) ADC. Significance of ASL perfusion changes at 2 weeks of PT2385 treatment was determined using a linear mixed model.

A logarithmic regression was used to fit the curve of EPO with trough PT2385 levels, whereas polynomial regression was used to fit the curve of EPO with reticulocytes. For PLA analyses, the Student *t* test was used to analyze for significant differences by patient in the number of HIF-1 and HIF-2 complexes between pretreatment and on-treatment tissue samples. GSEA for HIF-2 target genes (see ref. 16) was completed using the GSVA package (36) with the ssGSEA method. A mixed model was used to determine whether the expression estimates obtained were significantly different for pretreatment versus on-treatment patient biopsies from sensitive patients, using a compound symmetric covariance structure to account for correlation of estimates from the same patient. Heatmaps were created to visualize the expression of individual genes of the HIF-2 target gene signature.

Online content

Additional supplementary materials, additional references, source data, and clinical trial protocols are available online.

Results

To obtain insight into the mechanism of PT2385 action against ccRCC in humans, we implemented an IRB-approved protocol (UTSW STU 062015-063), enabling translational studies on patients at UTSW participating in the PT2385 phase I trial (NCT02293980). Among 51 patients from six institutions in the phase I trial, 26 patients enrolled in the dose-escalation phase and 25 in the dose-expansion. Eleven patients enrolled in the study at UTSW at the recommended phase II dose level or above, including 10 that participated in this companion study (**Table 1**). The patient population was extensively pretreated with a median number of 3.5 prior lines of therapy. Among these patients, 5 had stable disease for at least 4 months (median 6.9 months) and 5 had progressive disease. *VHL* was mutated in tumors from 5 of 9 patients for whom samples were available and *VHL* mutations were enriched among patients with stable disease. However, a *VHL* mutation was also found in a patient with progressive disease (**Table 1**).

Multiparametric MRI analyses

We explored the effects of PT2385 with mpMRI. We used ASL MRI to estimate tumor perfusion, which has been previously employed to evaluate antiangiogenic therapy (Supplementary Table S1; see Materials and Methods; refs. 37–41). Seven patients underwent mpMRI. We measured ASL perfusion at sites of metastases at baseline and following PT2385 initiation (**Fig. 1**). We correlated ASL changes with changes in tumor size. At 2 weeks, ASL perfusion decreased by 29% on average, but this was largely driven by changes in one patient (Pt45; **Fig. 1**; Supplementary Fig. S1A). We correlated maximal changes in ASL with time to progression and with one exception (Pt27), we found that greater reductions in ASL were associated with longer time to progression (Supplementary Fig. S1B).

Functional HIF-2 inhibition in nontumor tissues by PT2385

We evaluated the effects of PT2385 on EPO over time. EPO, which is secreted by kidney interstitial fibroblasts, is regulated by HIF-2 (42, 43) and may serve as a pharmacodynamic marker (15, 16). We observed a reduction in EPO at 2 weeks from baseline in 9 of 10 patients (**Fig. 1**;

Table 1. Summary of patients enrolled in phase I companion protocol.

Peloton ID	Internal patient reference[a]	Age (yrs)	Stage at diagnosis	Histology	Grade	*VHL* status	Lines of prior therapies	PT2385 concentration (D15) (μg/mL)	Percent EPO downregulation (2 weeks)	Percent reticulocyte downregulation (2 weeks)	mpMRI	Tumor samples[b]			Best response (RECIST)	PFS (days)
												Pretreatment	On-treatment	Progression		
11	(11)	47	III	Clear cell	3	mut	7	2.44	85	67	No	5[c]	2	22[c]	SD	604
18	(10)	65	IV	Clear cell	3	mut	5	0.49	83	N/A	No	2[c]	1[c]	8[c]	SD	167
23	(1)	57	N/A	Clear cell	N/A	wt	4	1.41	77	50	Yes	0	5	1[c]	PD	107
26	(2)	66	N/A	Clear cell	2	mut	5	0.8	65	50	Yes	1[c]	0	0	PD	40
27	(3)	64	IV	Clear cell	2	mut	2	1.21	70	27	Yes	4	4	5[c]	SD	220
34	(5)	72	I	Clear cell	2	wt	1	0.07	69	0	No	1[c]	0	0	PD	36
35	(6)	67	IV	Clear cell	4	wt	3	1.65	88	64	Yes	4	4	0	PD	36
42	(7)	70	III	Clear cell	1	N/A	2	2.33	77	60	Yes	0	0	0	SD	162
44	(8)	62	IV	Clear cell	N/A	wt	6	0.03[d]	5	0	Yes	4	0	0	PD	33
45	(9)	65	IV	Clear cell	3	mut	3	0.64	52	33	Yes	6[c]	4	9	SD	228

Abbreviations: D15, day 15; mut, mutant; N/A, not available (or applicable); PD, progressive disease; PFS, progression-free survival; SD, stable disease (for at least 4 months); wt, wild-type; yrs, age in years at start of trial.
[a]Used only for internal purposes.
[b]Sample number includes number of cores.
[c]Includes samples collected independently of study.
[d]Inadequate levels.

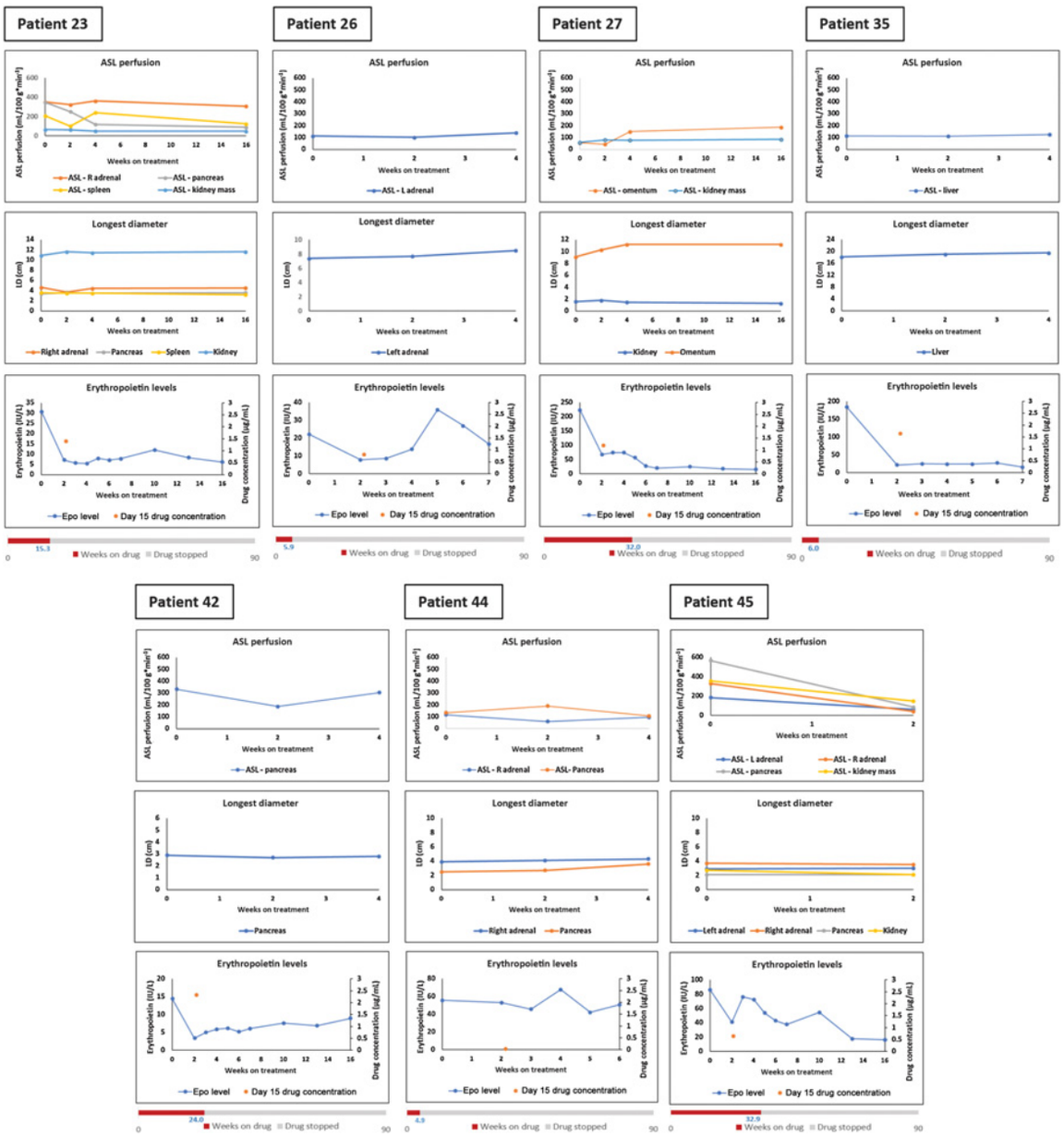

Figure 1.

Integrated mpMRI imaging, pharmacodynamic, and pharmacokinetic analyses in patients participating in phase I trial of PT2385. Arterial spin labeled (ASL) perfusion and longest diameter (LD) for the same target lesions at indicated time points following PT2385 administration. Erythropoietin is shown over time along with circulating drug concentrations at trough on day 15 (orange dot). Total weeks on treatment shown by the red bar (same scale across all patients).

Supplementary Fig. S1C). The reduction in EPO had a logarithmic correlation with PT2385 levels at trough ($R^2 = 0.58$; Supplementary Fig. S1D). The observed decrease in EPO was functionally significant, and EPO levels were associated with a reduction in red blood cell precursors, reticulocytes, through a quadratic relationship ($R^2 = 0.58$; Supplementary Fig. S1E). Although one caveat is that some EPO may be produced by some tumors, a reduction of tumor EPO by itself may not be expected to reduce reticulocyte counts, so it is likely that the effect observed is due to inhibition of HIF-2 in kidney interstitial fibroblasts.

In one patient (Pt44), EPO levels failed to decrease following PT2385 administration (**Fig. 1**). The patient received the recommended phase II dose (800 mg twice daily), but had the lowest trough levels of PT2385 across the whole cohort (0.03 μg/mL; **Fig. 1**; **Table 1**). Thus, failure to achieve sufficient drug concentration in this patient may account for the failure to inhibit HIF-2. Perhaps not surprisingly, there were no significant changes in ASL perfusion and this patient progressed quickly, remaining on drug for less than 5 weeks (**Fig. 1**). Overall, these data show that HIF-2 was inhibited in nontumor tissues in all but one patient, who likely achieved insufficient drug levels. Thus,

at least as determined by HIF-2 inhibition in nontumor tissues, adequate drug levels were achieved in all but one patient.

PT2385 specifically dissociates HIF-2 complexes in ccRCC metastases

To evaluate the effect of PT2385 on HIF-2 specifically in tumors, we leveraged on-treatment tumor biopsies. Pretreatment and on-treatment samples that were adequate were available for 3 patients (Pt27, Pt35, and Pt45). In all 3 patients, the same site was biopsied at baseline and while on drug, and importantly, the drug was not discontinued for the biopsy procedure. We asked whether PT2385 dissociated HIF2α/HIF1β heterodimers using a PLA. We used antibodies against HIF2α and HIF1β conjugated with complementary oligonucleotides, which can amplify a signal (detected by fluorescence microscopy) if they are in physical proximity. We readily detected HIF-2 complexes at baseline and observed a statistically significant decrease in HIF-2 complexes in 2 of the 3 patients (Pt27 and Pt45; **Fig. 2A**). In these 2 patients, we examined HIF-1 complexes in parallel (HIF1α/HIF1β). Similar levels of HIF-1 complexes were identified in pretreatment and on-treatment samples (Supplementary Fig. S2A). These data show that PT2385 dissociates HIF-2 complexes in patient metastases and that the effect is specific for HIF-2.

Inhibition of HIF-2 gene expression program by PT2385 in tumors

We next measured the impact of PT2385 on HIF-2–dependent gene expression by RNA-seq. We performed gene expression analyses in pretreatment and on-treatment biopsies. We previously defined the HIF-2–dependent transcriptome in renal cancer using tumorgrafts (16). RNA-seq analyses identified 296 genes downregulated by the inhibitor compared with vehicle-treated tumorgrafts. Eliminating noncoding RNAs and genes with unclear annotation reduced this list to 277 genes, which were used for gene set enrichment analysis (Supplementary Table S4). We observed a significant decrease in HIF-2 target genes in tumors from Pt27 and Pt45, but not Pt35 (**Fig. 2B**). Interestingly, this correlated with HIF-2 complex

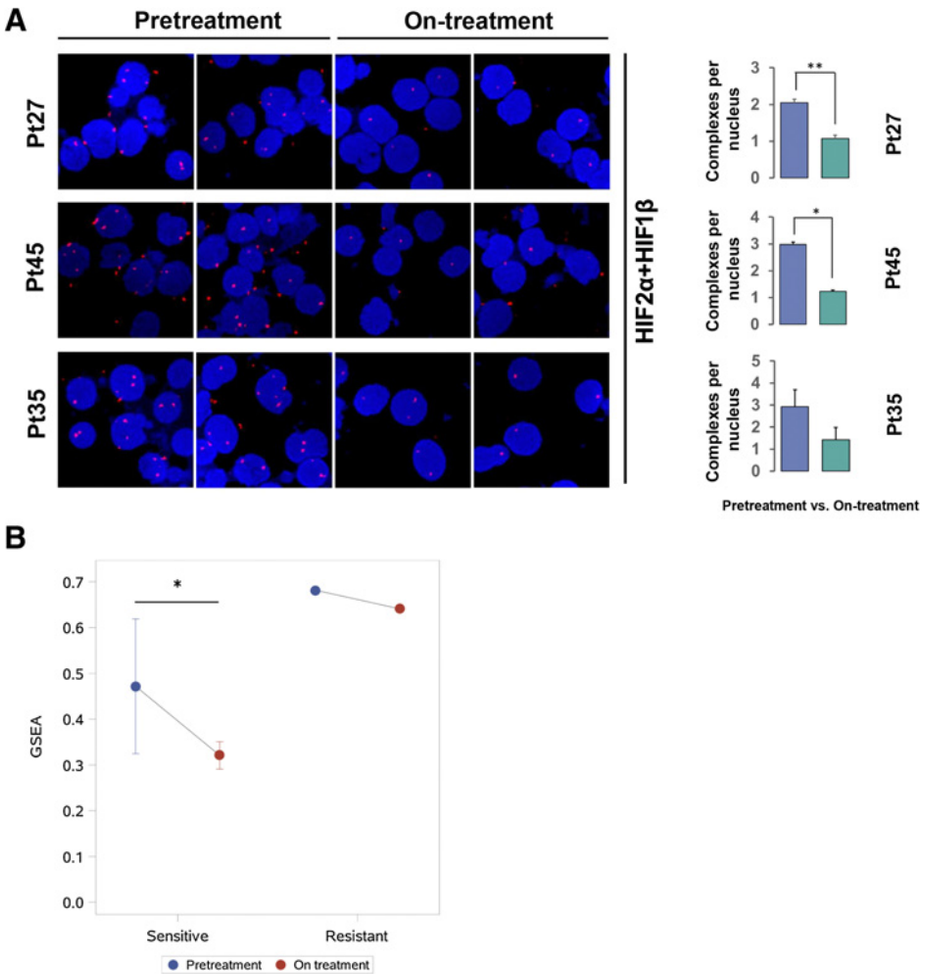

Figure 2.
PT2385 dissociates HIF-2 complexes inhibiting HIF-2 target genes. **A,** PLA of HIF2α/HIF1β complexes from touchpreps of biopsies from metastases of patients at week 6/7 of PT2385 (while receiving drug) compared with biopsies taken prior to treatment initiation for Pt27, Pt45, and Pt35. Representative images and quantitative data are shown. **B,** Gene set enrichment analysis for the HIF-2 target gene signature, comparing pretreatment versus week 6/7 biopsy samples from two sensitive patients (Pt27, Pt45) and one resistant patient (Pt35; *, $P < 0.05$; **, $P < 0.01$).

dissociation (**Fig. 2A**), and PT2385 activity in patients (**Table 1**). Although Pt27 and Pt45 derived prolonged benefit from PT2385 and remained on treatment for 32 and 32.9 weeks, respectively, Pt35 progressed after only 5 weeks (**Table 1**; **Fig. 1**). These data suggest that a reduction in HIF-2-dependent gene expression may be necessary for PT2385 antitumor activity.

Identification of an acquired resistance mutation in HIF2α reveals core HIF-2 dependency in ccRCC in humans

Pt11 enrolled in the dose-escalation part of the phase I trial in May 2015 and received 800 mg twice daily of PT2385, which became the recommended phase II dose (**Fig. 3A**). He had adequate circulating drug levels, as well as HIF-2 inhibition both in nontumor tissues (85% reduction in EPO with a 67% reduction in reticulocytes; see Supplementary Fig. S1C; **Table 1**) as well as in tumor tissues (Supplementary Fig. S2B). He remained on treatment for 87.1 weeks with stable disease by RECIST 1.1 (**Fig. 3B**; Supplementary Fig. S1C). This was remarkable as the patient had previously progressed on seven lines of systemic therapy including multiple VEGF/VEGFR2 inhibitors (16, 18). However, a mass in his remaining kidney (referred to as M4) progressed with increased enhancement, and in March 2016, it was biopsied (**Fig. 3A** and **B**; nontarget lesion #5).

First, we sought to determine whether M4 represented a metastasis, or an independent primary tumor arising in the remaining kidney. We performed WES and evaluated the mutations identified in M4 compared with other metastases from the same patient (Supplementary Table S5). Multiple mutations were shared across metastases, which indicated a shared origin (Supplementary Table S6). We then focused on mutations known to occur early during the process of RCC development. Mutations in both *VHL* and *PBRM1*, which were found in Pt11, are truncal mutations in ccRCC (44). The same *VHL* and *PBRM1* mutations found in M4 were found in previously collected M0 (abdominal wall), M1 (small bowel), and M2 (retroperitoneum) metastases, which showed that all these metastases (collected over a span of 6 years) arose from the same primary tumor (Supplementary Table S6).

Next, we sought to understand the mechanism of resistance. WES analyses of M4 identified a c.968G>A substitution in *HIF2A* (also called *EPAS1*). The mutation was detected in two tissue cores obtained during the same percutaneous CT-guided biopsy procedure (**Fig. 3C**; Supplementary Table S6). Although we did not have a pretreatment biopsy specifically for M4, the mutation was not observed in three other previously resected metastases (M0, M1, and M2; **Fig. 3D**; Supplementary Table S6). Overall, these data suggest that the mutation was acquired late, after exposure to PT2385.

Interestingly, this was the same mutation we had previously identified when we modeled resistance to HIF-2 inhibitors using the close analogue PT2399 in tumorgraft models (c.968G>A; ref. 16). For these experiments, tumorgraft-bearing mice (from a different patient) were treated with PT2399 for over 6 months, until resistance developed, and the tumors were then sequenced. Interestingly, the *HIF2A* c.968G>A mutation translates to a p.Gly323Glu, and Gly323 lies in the pocket bound by PT2385 and would be expected to interfere with drug binding (16).

Gatekeeper mutation preserves HIF-2 complexes and gene expression

We hypothesized that if the HIF2α G323E mutation functioned as a gatekeeper, HIF-2 complexes should be preserved in the resistant kidney metastases, and performed PLA assays. Importantly, as for other on-study biopsies, the procedure was performed while the patient remained on drug. As shown in **Fig. 3E**, the number of HIF-2 complexes detected in M4 was similar to an untreated metastasis (M0). Thus, we conclude that the G323E substitution prevented HIF-2 dissociation by PT2385 in the renal metastasis. These results are in keeping with previous results in cells in culture showing that ectopic expression of HIF2α G323E is sufficient to prevent drug-induced dissociation of HIF-2 complexes (16). This mutation has also been shown to interfere with drug binding in biochemical experiments (45). Overall, these data show for the first time in humans that resistance to PT2385 treatment arises from the development of a gatekeeper mutation in HIF2α.

Next, we examined the effects of the G323E mutation on HIF-2 target gene expression by RNA-seq. We focused on genes downregulated by the HIF-2 inhibitor in a tumorgraft line that had been generated from this particular patient (see Materials and Methods). Out of 277 genes evaluated (representing the HIF2α gene signature), 170 were downregulated in tumorgrafts upon treatment with the related HIF-2 inhibitor PT2399 (Supplementary Table S7). To extrapolate from mouse tumorgrafts, we narrowed the list by requiring that the expression of these genes be increased in an untreated tumor from the patient (M0), which left 116 genes (**Fig. 3F**; Supplementary Table S7). This list corresponds to genes expressed in the patient tumor that are downregulated upon treatment with the HIF-2 inhibitor in corresponding tumorgrafts. We then evaluated the 116 genes in the M4 metastasis with the HIF2α G323E mutation. We found that over 40% of the genes were expressed at levels comparable with control samples and were not downregulated by PT2385 ($n = 48$; **Fig. 3F**; Supplementary Table S7). The results, which may have been confounded by stromal contamination of the M4 biopsy samples, were highly statistically significant ($P < 0.0001$). Furthermore, among the 48 genes, 21 were expressed at levels comparable with untreated samples including several canonical HIF-2 target genes such as *IGFBP1, LOX*, and *SERPINE1* (**Fig. 3F**; Supplementary Table S7). Overall, these data show that the HIF2α G323E mutation interferes with PT2385-mediated inhibition of HIF-2 target genes in the resistant metastases.

Notably, we identified the same *HIF2A* mutation (c.968G>A; p.G323E) in a second patient, Pt35 (Supplementary Table S8). As for Pt11, Pt35 had adequate circulating drug levels and HIF-2 inhibition in nontumor tissues (**Fig. 1**; **Table 1**). However, the finding of a *HIF2A* mutation in Pt35 was unexpected. Pt35 had progression after just 36 days on drug (Supplementary Fig. S3A; **Table 1**), which was more in keeping with innate resistance, which we believed to evidence HIF-2–independent biology. In fact, the biopsy showing the mutation was the week 6/7 on-treatment biopsy, which became the progression biopsy. Similarly unexpected was the finding that the mutation was absent from the pretreatment biopsy, which was of the same site where the week 6/7 biopsy was obtained (a liver metastasis; Supplementary Fig. S3B; Supplementary Table S8). We reviewed other mutations and while some mutations, such as in *TSC1*, were observed across pretreatment and on-treatment/progression samples, others, such as a *PBRM1* mutation, were only called by our algorithm in the progression samples (Supplementary Table S8). Manual review of the BAM files showed the *PBRM1* mutation in both pretreatment and progression samples (Supplementary Fig. S3C and S3D), but the mutation was present at low frequency and thus not called by our algorithm. Although the *HIF2A* mutation was found in a progression biopsy at significantly higher frequencies than the *TSC1* and *PBRM1* mutations, we cannot exclude the possibility that our

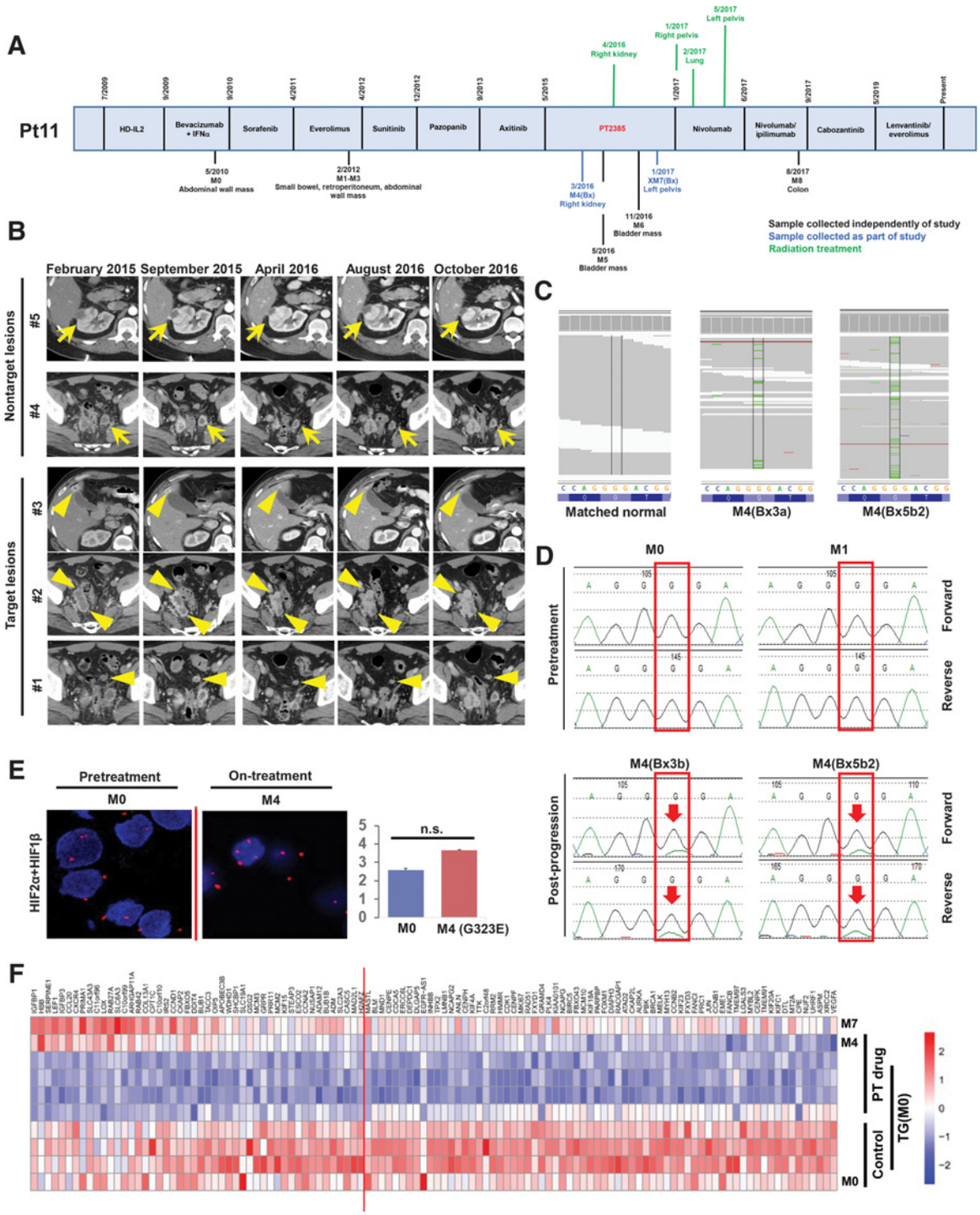

Figure 3.

Identification of a resistance mutation with preserved HIF-2 complex formation and target gene expression despite PT2385 treatment in a patient metastasis. **A,** Pt11 treatment timeline including tumor resections and biopsies. A tumorgraft (PDX model) referred to as XP165 was generated from M0. Subsequently resected or biopsied metastases were designated M1–8. Treatment with the HIF-2 inhibitor (PT2385) spanned from May 2015 to January 2017. **B,** CT images of target and nontarget (including biopsied metastasis, #5) at indicated times. **C,** WES reads of M4 biopsies (2 cores) showing in green the *HIF2A* (*EPAS1*) 968G>A substitution compared with a matched normal sample from the same patient. **D,** Sanger sequencing analyses showing small 968G>A mutant peaks in M4 biopsies compared with reference samples predating PT2385 treatment [M1 and a tumorgraft derived from M0 (T(M0)_TGc1(8133))]. **E,** PLA of HIF2α/HIF1β heterodimers in pretreatment metastasis (M0) and metastasis with resistance mutation (M4) with quantitation. **F,** Heatmap of HIF-2 signature genes in untreated patient metastasis (M0) as well as tumorgrafts (TG) untreated/vehicle treated (control); followed by treated tumorgrafts and patient tumor biopsy sample with resistance mutation (M4; under PT drug); and finally a post-trial tumor sample (M7). Red line indicates cutoff for the 48 genes downregulated by the HIF-2 inhibitor, but preserved in mutant M4 biopsy sample. n.s., nonstatistically significant.

failure to detect it in the pretreatment sample (even by manual review; Supplementary Fig. S3B) is due to tumor heterogeneity and potentially tumor contamination by stromal or other cells. As the probability that this mutation would be an acquired mutation not preexisting in the metastasis seems low (given the short time to progression), we favor this option. Independently, the presence of this mutation likely explains the persistence of HIF-2 complexes and preserved HIF-2 target gene expression despite PT2385 treatment (**Fig. 2A** and **B**). Overall, these data show that rapid acquisition of resistance may not always indicate target-independent biology and raises the possibility that resistance mutations may preexist in tumors of some patients at low frequency.

Other potential mechanisms of resistance

We had suitable samples to evaluate resistance for one other patient, Pt27. Pt27 achieved appropriate circulating drug levels and HIF-2 inhibition in nontumor tissues (**Fig. 1**; **Table 1**). He was sensitive to the HIF-2 inhibitor and remained free of progression for 220 days (**Table 1**; Supplementary Fig. S4A). WES analyses of a site of progression failed to identify mutations in *HIF2A* (or *HIF1B*, which we previously also linked to resistance in tumorgraft models; ref. 16). Tantalizingly, we identified a *TP53* mutation (c.818G>A; p.R273H; Supplementary Fig. S4B; Supplementary Table S9). The p53 R273H mutation is a well-validated tumor-associated mutation extensively reported as somatically acquired in tumors (https://cancer.sanger.ac.uk/cosmic). Although the mutation was significantly enriched in the progression biopsy compared with pretreatment and on-treatment biopsies (Supplementary Fig. S4B), the interpretation was confounded by the fact that pretreatment and on-treatment biopsies had scant tumor cells (as determined also by the evaluation of *VHL* and *PBRM1* mutations; see Supplementary Table S9 and Supplementary Fig. S4C). To assess whether the mutation may be acquired, we turned to IHC. *TP53* mutations are often associated with protein stabilization, which can be scored by IHC. p53 IHC analyses showed low signal in tumor cells in the pretreatment biopsy sample, and high signal in two progression biopsy cores from the same progression metastasis (Supplementary Fig. S4D). Overall, these data are consistent with the notion that the *TP53* mutation was acquired coincidentally with the development of resistance, and raise the possibility that p53, as previously postulated on the basis of cell line analyses in tissue culture (17), may also be implicated in resistance to HIF-2 inhibitors. However, further studies will be required to demonstrate definitively the potential role of p53 in this context.

Discussion

We report the results of extensive translational studies in patients participating in a first-in-human, first-in-class clinical trial of the HIF-2 inhibitor, PT2385. Using a combination of approaches, we show for the first time in humans that PT2385 inhibited HIF-2 not only in normal tissues, but also in metastases, leading to the dissociation of HIF-2 heterodimers and the inhibition of HIF-2 target genes. We report that prolonged treatment with PT2385 resulted in the acquisition of a gatekeeper mutation preventing HIF-2 dissociation and preserving HIF-2 gene expression despite drug treatment. The identification of an acquired resistance mutation validates HIF-2 as the drug target in patients. Interestingly, the same mutation was found in a second patient, who developed resistance shortly after initiation of treatment. These results raise the possibility that some patients who may ordinarily be regarded as having innate resistance, which would be in keeping with HIF-2–independent biology, may still have a core HIF-2 dependency. More importantly, these data establish a hard-wired dependency on HIF-2 for ccRCC tumorigenesis.

The situation is akin to EGFR mutations in lung cancer, where the acquisition of resistance mutations reveals a persistent dependency on EGFR activity, which can be targeted with subsequent generation inhibitors (46, 47). The HIF-2 dependency/therapeutic vulnerability is likely to be similarly acquired early during tumor development, which is believed to start with inactivation of the *VHL* gene (48, 49). The data show that HIF-2 is a valid target in ccRCC and paves the way for future inhibitors. Drugs like PT2977 (MK-6482), a second-generation oral inhibitor with more predictable absorption, and which binds the same pocket, are likely to be similarly affected by the same resistance mutations. However, other vulnerabilities have been identified in the protein (45, 50), and HIF2α may be targeted through approaches other than small-molecule allosteric inhibitors.

The finding of the HIF2α p.G323E mutation in a progressing metastasis after 6 weeks of treatment in Pt35 raises the strong suspicion that the mutation preexisted (even if it could not be detected) prior to the initiation of PT2385. Furthermore, it suggests that the mutation may have been present in more than just a few cells. Most likely the mutation was a passenger mutation. However, the possibility exists that such a mutation could have been selected for if it afforded a growth advantage. This might be the case if the HIF2α drug-binding cavity were to be bound also by an endogenous ligand that dampened HIF2α activity and which could be similarly blocked by the mutation. However, a search of the COSMIC database for the HIF2α p.G323E mutation fails to reveal other mutations besides the one we previously reported in tumorgrafts (16), which makes this possibility less likely.

That the same resistance mutation (HIF2α, p.G323E) had been previously identified in a preclinical tumorgraft model of acquired resistance from a different patient (16) is in keeping with the notion that tumorgrafts are valid models to study acquired resistance in humans. Accordingly, we speculate that a second resistance mutation we identified in tumorgrafts, a mutation in HIF1β (p.F446L; ref. 16), which increases the binding affinity for HIF2α (45), may eventually also be found in humans.

There may be other mechanisms of resistance. The finding of a canonical *TP53* mutation in a progression sample suggests that p53 may also be involved in resistance. Interestingly, experiments in RCC cell lines in culture suggested that *TP53* mutations may confer resistance to HIF-2 inhibitors (17). However, the extent to which *TP53* mutations result in resistance remains to be determined, and our previous studies in tumorgrafts showed that p53-mutant tumors (i.e. XP374) may still be inhibited by HIF-2 inhibitors (16).

Finally, it remains unclear why some VHL-deficient tumors do not respond to HIF-2 inhibitors. We previously showed in tumorgrafts that tumor inhibition correlated with HIF2α protein levels and that tumors that expressed low levels of HIF2α do not respond (16). Some of these ccRCCs express HIF1α, but whether HIF1α is a driver in some ccRCCs remains to be determined, and although both HIF-2 and HIF-1 promote *VEGFA* expression (51), some data suggest that HIF-1 may function as a tumor suppressor gene in ccRCC (5, 52).

Overall, these data show that PT2385 inhibits HIF-2 in ccRCC in humans, revealing a core tumor dependency that could be further exploited.

Disclosure of Potential Conflicts of Interest

K.D. Courtney reports receiving other commercial research support and is an advisory board member/unpaid consultant for Peloton Therapeutics. A.J. Madhuranthakam reports receiving other commercial research support from Philips Healthcare and is an employee/paid consultant for and holds ownership interest (including patents) in UT Southwestern Medical Center. Y. Arriaga is an employee/paid consultant for IBM Watson Health. S. Kalva is an employee/paid consultant for Medtronic Inc., Koo Foundation, Dova Pharmaceuticals, and US Vascular; holds ownership interest (including patents) in Altheae Health; and has received Royalties from Springer and Elsevier for book chapters/books, consulting fee from Medtronic Inc., Koo Foundation, Dova Pharmaceuticals, and US Vascular, speaker fee from Penumbra Inc., and personal fee for expert testimony on a legal case. B.I. Rini is an employee/paid consultant for and reports receiving commercial research grants from Peloton and Merck. I. Pedrosa reports receiving other commercial research support from Philips Healthcare, reports receiving speakers bureau honoraria from Bayer Healthcare, and holds ownership interest (including patents) in Philips Healthcare. J. Brugarolas is an employee/paid consultant for Exelixis, Arrowhead, and Bethyl; reports receiving commercial research grants from Arrowhead; and holds ownership interest (including patents) in Peloton Therapeutics/Merck. No potential conflicts of interest were disclosed by the other authors.

Authors' Contributions

Conception and design: K.D. Courtney, S. Zhang, B.I. Rini, I. Pedrosa, J. Brugarolas
Development of methodology: K.D. Courtney, A.J. Madhuranthakam, Q. Yuan, R.A. Figlin, I. Pedrosa, J. Brugarolas
Acquisition of data (provided animals, acquired and managed patients, provided facilities, etc.): K.D. Courtney, Y. Ma, A. Diaz de Leon, A. Joyce, H. Hill, A.J. Madhuranthakam, Q. Yuan, Y. Zhang, J. Chang, O. Fatunde, Y. Arriaga, A.E. Frankel, S. Kalva, R.A. Figlin, B.I. Rini, P. Kapur, I. Pedrosa, J. Brugarolas
Analysis and interpretation of data (e.g., statistical analysis, biostatistics, computational analysis): K.D. Courtney, Y. Ma, A. Diaz de Leon, A. Christie, Z. Xie, N. Singla, A.J. Madhuranthakam, Q. Yuan, Y. Xi, Y. Zhang, Y. Arriaga, S. Zhang, O. Reig Torras, R.A. Figlin, B.I. Rini, T. Wang, I. Pedrosa, J. Brugarolas
Writing, review, and/or revision of the manuscript: K.D. Courtney, Y. Ma, A. Diaz de Leon, A. Christie, L. Woolford, N. Singla, A.J. Madhuranthakam, Q. Yuan, Y. Xi, Y. Zhang, Y. Arriaga, S. Kalva, S. Zhang, R.A. Figlin, B.I. Rini, R.M. McKay, T. Wang, I. Pedrosa, J. Brugarolas
Administrative, technical, or material support (i.e., reporting or organizing data, constructing databases): K.D. Courtney, Y. Ma, A. Diaz de Leon, Z. Xie, L. Woolford, A. Joyce, A.J. Madhuranthakam, J. Chang, P. Kapur, J. Brugarolas
Study supervision: K.D. Courtney, R.A. Figlin, I. Pedrosa, J. Brugarolas
Other (performed all of the histologic duties): T. McKenzie

Acknowledgments

This manuscript is dedicated to the memory of Richard Martinez, who made extensive contributions to advance our understanding of the disease. We thank the patients who generously participated in the studies reported here. We are particularly grateful to those patients consenting to tumor biopsies to advance scientific research, along with their families. We thank Peloton Therapeutics for agreeing to the study and sharing data. This work was supported by Cancer Prevention and Research Institute of Texas grants RP160440 (to J. Brugarolas), and NIH Grants P50CA196516 (to J. Brugarolas, K.D. Courtney, P. Kapur, R. McKay, I. Pedrosa, T. Wang), R01CA154475 (to I. Pedrosa, P. Kapur), U01CA207091 (to A.J. Madhuranthakam, I. Pedrosa), and R03ES026397-01 (to T. Wang). K. Courtney received support from NIH/NCATS KL2TR001103. N. Singla receives support from the Ruth L. Kirschstein National Research Service Award T32 CA136515-09. O. Reig Torras receives support from BECA FSEOM/FUNDACION CRIS CONTRA EL CANCER 2018. Histology equipment was purchased with funding from the National Center for Advancing Translational Sciences (Center for Translational Medicine UL1TR001105). The authors would like to acknowledge the UT Southwestern Tissue Resource Research and the UT Southwestern Small Animal Imaging Resource, which are supported in part by the Harold C. Simmons Cancer Center through an NCI Cancer Center Support Grant (P30CA142543).

The costs of publication of this article were defrayed in part by the payment of page charges. This article must therefore be hereby marked *advertisement* in accordance with 18 U.S.C. Section 1734 solely to indicate this fact.

Received May 6, 2019; revised August 16, 2019; accepted November 5, 2019; published first November 14, 2019.

References

1. Nickerson ML, Jaeger E, Shi Y, Durocher JA, Mahurkar S, Zaridze D, et al. Improved identification of von Hippel-Lindau gene alterations in clear cell renal tumors. Clin Cancer Res 2008;14:4726–34.
2. Simon MC. The hypoxia response pathways - hats off! N Engl J Med 2016;375:1687–9.
3. Giaccia AJ, Simon MC, Johnson R. The biology of hypoxia: the role of oxygen sensing in development, normal function, and disease. Genes Dev 2004;18:2183–94.
4. Gordan JD, Bertout JA, Hu CJ, Diehl JA, Simon MC. HIF-2α promotes hypoxic cell proliferation by enhancing c-myc transcriptional activity. Cancer Cell 2007;11:335–47.
5. Raval RR, Lau KW, Tran MG, Sowter HM, Mandriota SJ, Li JL, et al. Contrasting properties of hypoxia-inducible factor 1 (HIF-1) and HIF-2 in von Hippel-Lindau-associated renal cell carcinoma. Mol Cell Biol 2005;25:5675–86.
6. Shen C, Kaelin WG Jr. The VHL/HIF axis in clear cell renal carcinoma. Semin Cancer Biol 2013;23:18–25.
7. Bruick RK, McKnight SL. Building better vasculature. Genes Dev 2001;15:2497–502.
8. Ferrara N, Hillan KJ, Gerber HP, Novotny W. Discovery and development of bevacizumab, an anti-VEGF antibody for treating cancer. Nat Rev Drug Discov 2004;3:391–400.
9. Choueiri TK, Motzer RJ. Systemic therapy for metastatic renal-cell carcinoma. N Engl J Med 2017;376:354–66.
10. Covello KL, Kehler J, Yu H, Gordan JD, Arsham AM, Hu CJ, et al. HIF-2α regulates Oct-4: effects of hypoxia on stem cell function, embryonic development, and tumor growth. Genes Dev 2006;20:557–70.
11. Koehler AN. A complex task? Direct modulation of transcription factors with small molecules. Curr Opin Chem Biol 2010;14:331–40.
12. Rogers JL, Bayeh L, Scheuermann TH, Longgood J, Key J, Naidoo J, et al. Development of inhibitors of the PAS-B domain of the HIF-2α transcription factor. J Med Chem 2013;56:1739–47.
13. Scheuermann TH, Tomchick DR, Machius M, Guo Y, Bruick RK, Gardner KH. Artificial ligand binding within the HIF2α PAS-B domain of the HIF2 transcription factor. Proc Natl Acad Sci U S A 2009;106:450–5.
14. Scheuermann TH, Li Q, Ma HW, Key J, Zhang L, Chen R, et al. Allosteric inhibition of hypoxia inducible factor-2 with small molecules. Nat Chem Biol 2013;9:271–6.
15. Wallace EM, Rizzi JP, Han G, Wehn PM, Cao Z, Du X, et al. A small-molecule antagonist of HIF2α is efficacious in preclinical models of renal cell carcinoma. Cancer Res 2016;76:5491–500.
16. Chen W, Hill HM, Christie A, Kim MS, Holloman E, Pavia-Jimenez A, et al. Targeting renal cell carcinoma with a HIF-2 antagonist. Nature 2016;539:112–7.
17. Cho H, Du X, Rizzi JP, Liberzon E, Chakraborty AA, Gao W, et al. On-target efficacy of a HIF-2α antagonist in preclinical kidney cancer models. Nature 2016;539:107–11.
18. Courtney KD, Infante JR, Lam ET, Figlin RA, Rini BI, Brugarolas J, et al. Phase I dose-escalation trial of PT2385, a first-in-class hypoxia-inducible factor-2α antagonist in patients with previously treated advanced clear cell renal cell carcinoma. J Clin Oncol 2018;36:867–74.
19. Robson PM, Madhuranthakam AJ, Dai W, Pedrosa I, Rofsky NM, Alsop DC. Strategies for reducing respiratory motion artifacts in renal perfusion imaging with arterial spin labeling. Magn Reson Med 2009;61:1374–87.
20. Tofts PS. Modeling tracer kinetics in dynamic Gd-DTPA MR imaging. J Magn Reson Imaging 1997;7:91–101.
21. Pavia-Jimenez A, Tcheuyap VT, Brugarolas J. Establishing a human renal cell carcinoma tumorgraft platform for preclinical drug testing. Nat Protoc 2014;9:1848–59.

22. Sivanand S, Pena-Llopis S., Zhao H, Kucejova B, Spence P, Pavia-Jimenez A, et al. A validated tumorgraft model reveals activity of dovitinib against renal cell carcinoma. Sci Transl Med 2012;4:137ra75.
23. Li H, Durbin R. Fast and accurate short read alignment with Burrows-Wheeler transform. Bioinformatics 2009;25:1754–60.
24. DePristo MA, Banks E, Poplin R, Garimella KV, Maguire JR, Hartl C, et al. A framework for variation discovery and genotyping using next-generation DNA sequencing data. Nat Genet 2011;43:491–8.
25. McKenna A, Hanna M, Banks E, Sivachenko A, Cibulskis K, Kernytsky A, et al. The Genome Analysis Toolkit: a MapReduce framework for analyzing next-generation DNA sequencing data. Genome Res 2010;20: 1297–303.
26. Van der Auwera GA, Carneiro MO, Hartl C, Poplin R, Del Angel G, Levy-Moonshine A, et al. From FastQ data to high confidence variant calls: the Genome Analysis Toolkit best practices pipeline. Curr Protoc Bioinform 2013; 43:1–33.
27. Chiang C, Layer RM, Faust GG, Lindberg MR, Rose DB, Garrison EP, et al. SpeedSeq: ultra-fast personal genome analysis and interpretation. Nat Methods 2015;12:966–8.
28. Cibulskis K, Lawrence MS, Carter SL, Sivachenko A, Jaffe D, Sougnez C, et al. Sensitive detection of somatic point mutations in impure and heterogeneous cancer samples. Nat Biotechnol 2013;31:213–9.
29. Koboldt DC, Zhang Q, Larson DE, Shen D, McLellan MD, Lin L, et al. VarScan 2: somatic mutation and copy number alteration discovery in cancer by exome sequencing. Genome Res 2012;22:568–76.
30. Saunders CT, Wong WS, Swamy S, Becq J, Murray LJ, Cheetham RK. Strelka: accurate somatic small-variant calling from sequenced tumor-normal sample pairs. Bioinformatics 2012;28:1811–7.
31. Wang K, Li M, Hakonarson H. ANNOVAR: functional annotation of genetic variants from high-throughput sequencing data. Nucleic Acids Res 2010;38: e164.
32. Wang T, Bu CH, Hildebrand S, Jia G, Siggs OM, Lyon S, et al. Probability of phenotypically detectable protein damage by ENU-induced mutations in the Mutagenetix database. Nat Commun 2018;9:441.
33. Dobin A, Davis CA, Schlesinger F, Drenkow J, Zaleski C, Jha S, et al. STAR: ultrafast universal RNA-seq aligner. Bioinformatics 2013;29: 15–21.
34. Liao Y, Smyth GK, Shi W. featureCounts: an efficient general purpose program for assigning sequence reads to genomic features. Bioinformatics 2014;30:923–30.
35. Barbie DA, Tamayo P, Boehm JS, Kim SY, Moody SE, Dunn IF, et al. Systematic RNA interference reveals that oncogenic KRAS-driven cancers require TBK1. Nature 2009;462:108–12.
36. Hanzelmann S, Castelo R, Guinney J. GSVA: gene set variation analysis for microarray and RNA-seq data. BMC Bioinform 2013;14:7.
37. Bharwani N, Miquel ME, Powles T, Dilks P, Shawyer A, Sahdev A, et al. Diffusion-weighted and multiphase contrast-enhanced MRI as surrogate markers of response to neoadjuvant sunitinib in metastatic renal cell carcinoma. Br J Cancer 2014;110:616–24.
38. de Bazelaire C, Alsop DC, George D, Pedrosa I, Wang Y, Michaelson MD, et al. Magnetic resonance imaging-measured blood flow change after antiangiogenic therapy with PTK787/ZK 222584 correlates with clinical outcome in metastatic renal cell carcinoma. Clin Cancer Res 2008;14:5548–54.
39. Flaherty KT, Rosen MA, Heitjan DF, Gallagher ML, Schwartz B, Schnall MD, et al. Pilot study of DCE-MRI to predict progression-free survival with sorafenib therapy in renal cell carcinoma. Cancer Biol Ther 2008;7:496–501.
40. Hahn OM, Yang C, Medved M, Karczmar G, Kistner E, Karrison T, et al. Dynamic contrast-enhanced magnetic resonance imaging pharmacodynamic biomarker study of sorafenib in metastatic renal carcinoma. J Clin Oncol 2008; 26:4572–8.
41. Schor-Bardach R, Alsop DC, Pedrosa I, Solazzo SA, Wang X, Marquis RP, et al. Does arterial spin-labeling MR imaging-measured tumor perfusion correlate with renal cell cancer response to antiangiogenic therapy in a mouse model? Radiology 2009;251:731–42.
42. Rankin EB, Biju MP, Liu Q, Unger TL, Rha J, Johnson RS, et al. Hypoxia-inducible factor-2 (HIF-2) regulates hepatic erythropoietin in vivo. J Clin Invest 2007;117:1068–77.
43. Scortegagna M, Ding K, Zhang Q, Oktay Y, Bennett MJ, Bennett M, et al. HIF-2α regulates murine hematopoietic development in an erythropoietin-dependent manner. Blood 2005;105:3133–40.
44. Gerlinger M, Horswell S, Larkin J, Rowan AJ, Salm MP, Varela I, et al. Genomic architecture and evolution of clear cell renal cell carcinomas defined by multi-region sequencing. Nat Genet 2014;46:225–33.
45. Wu D, Su X, Lu J, Li S, Hood BL, Vasile S, et al. Bidirectional modulation of HIF-2 activity through chemical ligands. Nat Chem Biol 2019;15:367–76.
46. Finlay MR, Anderton M, Ashton S, Ballard P, Bethel PA, Box MR, et al. Discovery of a potent and selective EGFR inhibitor (AZD9291) of both sensitizing and T790M resistance mutations that spares the wild type form of the receptor. J Med Chem 2014;57:8249–67.
47. Kobayashi Y, Togashi Y, Yatabe Y, Mizuuchi H, Jangchul P, Kondo C, et al. EGFR Exon 18 mutations in lung cancer: molecular predictors of augmented sensitivity to afatinib or neratinib as compared with first- or third-generation TKIs. Clin Cancer Res 2015;21:5305–13.
48. Gerlinger M, Rowan AJ, Horswell S, Larkin J, Endesfelder D, Gronroos E, et al. Intratumor heterogeneity and branched evolution revealed by multiregion sequencing. N Engl J Med 2012;366:883–92.
49. Turajlic S, Xu H, Litchfield K, Rowan A, Horswell S, Chambers T, et al. Deterministic evolutionary trajectories influence primary tumor growth: TRACERx renal. Cell 2018;173:595–610.
50. Wu D, Potluri N, Lu J, Kim Y, Rastinejad F. Structural integration in hypoxia-inducible factors. Nature 2015;524:303–8.
51. Hu CJ, Wang LY, Chodosh LA, Keith B, Simon MC. Differential roles of hypoxia-inducible factor 1α (HIF-1α) and HIF-2α in hypoxic gene regulation. Mol Cell Biol 2003;23:9361–74.
52. Shen C, Beroukhim R, Schumacher SE, Zhou J, Chang M, Signoretti S, et al. Genetic and functional studies implicate HIF1α as a 14q kidney cancer suppressor gene. Cancer Discov 2011;1:222–35.